

# Truncated Diffusion Probabilistic Models

Huangjie Zheng<sup>1,2</sup>, Pengcheng He<sup>2</sup>, Weizhu Chen<sup>2</sup>, Mingyuan Zhou<sup>1</sup>

huangjie.zheng@utexas.edu, penhe@microsoft.com,  
wzchen@microsoft.com, mingyuan.zhou@mccombs.utexas.edu

The University of Texas at Austin<sup>1</sup> Microsoft Azure AI<sup>2</sup>

## Abstract

Employing a forward Markov diffusion chain to gradually map the data to a noise distribution, diffusion probabilistic models learn how to generate the data by inferring a reverse Markov diffusion chain to invert the forward diffusion process. To achieve competitive data generation performance, they demand a long diffusion chain that makes them computationally intensive in not only training but also generation. To significantly improve the computation efficiency, we propose to truncate the forward diffusion chain by abolishing the requirement of diffusing the data to random noise. Consequently, we start the inverse diffusion chain from an implicit generative distribution, rather than a random noise, and learn its parameters by matching it to the distribution of the data corrupted by the truncated forward diffusion chain. Experimental results show our truncated diffusion probabilistic models provide consistent improvements over the non-truncated ones in terms of the generation performance and the number of required inverse diffusion steps.

## 1 Introduction

Gaussian diffusion-based (or score-based) generative models have recently achieved impressive performance on several commonly used image generation benchmarks (Song & Ermon, 2019; Ho et al., 2020; Song & Ermon, 2020; Song et al., 2021b; Dhariwal & Nichol, 2021), surpassing many existing deep generative models, such as autoregressive models (Van den Oord et al., 2016), variational auto-encoders (VAEs) (Kingma & Welling, 2013; Rezende et al., 2014; Van Den Oord et al., 2017; Razavi et al., 2019), and generative adversarial networks (GANs) (Goodfellow et al., 2014; Radford et al., 2015; Arjovsky et al., 2017; Miyato et al., 2018; Brock et al., 2019; Karras et al., 2019, 2020b).

Diffusion probabilistic models (Sohl-Dickstein et al., 2015) are a class of generative models that first define a forward (or inference) diffusion process to transform the data distribution into a tractable noise distribution, and then infer an inverse (or generative) diffusion process to define how to regenerate the data starting from that noise distribution. Related to this modeling framework but independently developed through the lens of score matching (Hyvärinen & Dayan, 2005; Vincent, 2011) and Langevin dynamics (Neal, 2011; Welling & Teh, 2011), noise conditional score networks introduced by Song & Ermon (2019) have delivered surprisingly promising results in image generation. An apparent similarity shared between diffusion probabilistic models and score-based ones is corrupting data with noise at various scales. Looking beyond that similarity, Ho et al. (2020) reveal the close connections between these two modeling frameworks and show that, with appropriate parameterization and network architectures, the Gaussian distribution based denoising diffusion probabilistic models (DDPMs) are also capable of generating high-quality image samples. The score-based generative models and diffusion-based ones have been further unified by Song et al. (2021b) from the viewpoint of discretized stochastic differential equations.

While Gaussian diffusion-based generative models have shown promising generation ability, they are notorious for requiring intensive computation in not only training the model, but also sampling from the trained model. For example, as pointed out in Song et al. (2020), “it takes around 20 hours to sample 50k images of size  $32 \times 32$  from a DDPM, but less than a minute to do so from a GAN on a Nvidia 2080 Ti GPU.” This high computation cost is mainly attributed to the need of performing hundreds or even thousands of Gaussian

diffusion steps under both the forward and inverse Gaussian Markov diffusion chains, severely limiting their use in real-world applications.

To address this computational complexity issue, several techniques have been proposed to reduce the number of Gaussian diffusion steps, such as introducing non-Markovian diffusion processes (Song et al., 2020; Kong & Ping, 2021), adaptive noise scheduling (San-Roman et al., 2021), and knowledge distillation (Luhman & Luhman, 2021). However, due to the fact that the Gaussian assumption in the denoising diffusion steps only holds in the limit of small diffusion rate (Feller, 1949; Sohl-Dickstein et al., 2015), these existing works still cannot significantly reduce the number of required diffusion steps, at least not by orders of magnitude.

The fundamental challenge faced by previous strategies is that when the diffusion process is limited to a small number of steps, the diffusion rate will become too large to allow the Gaussian assumption of every denoising diffusion step to hold. To address this challenge, we introduce truncated diffusion probabilistic modeling (TDPM) that keeps small diffusion rates while no longer requiring the forward Markov diffusion chain to transform the data into a tractable (*e.g.*, Gaussian) distribution. This allows one to shorten the diffusion trajectory to an arbitrary length, at the expense of requiring the inverse diffusion process to start from a distribution that is no longer tractable and needs to be learned from the training data.

In TDPM, we truncate the forward Gaussian diffusion chain of an existing diffusion probabilistic model like DDPM (Ho et al., 2020), which is originally designed to employ many steps to diffuse the data into a Gaussian noise. With the truncated chain, TDPM no longer diffuses the data into a tractable noise distribution but still keeps the diffusion rates small. Consequently, in TDPM, the outcome of the truncated forward diffusion chain is no longer a Gaussian distribution when the truncation level is high. At the start of the inverse diffusion chain, TDPM focuses on closing the gap between this output and a usual Gaussian assumption. Concretely, our proposed solution is to use an implicit generative distribution transformed from Gaussian noise to model the outcome distribution of the truncated diffusion chain. With the help of this implicit distribution, in the inverse diffusion chain we can start from the truncated point and substantially improve the sampling efficiency. We show that simply keeping the original setting of an existing diffusion model like DDPM, the proposed TDPM only needs to learn an implicit generative distribution to match the corrupted data distribution under the truncated chain. This implicit generative distribution can be realized by either adding a new generator or utilizing the same U-Net used by DDPM in its reverse diffusion. The first choice has a higher modeling flexibility, while the second one adds no extra parameters into generation.

Our main contributions are summarized as follows:

- We propose TDPM to substantially reduce the number of required diffusion steps by learning an implicit distribution to start the inverse diffusion chain.
- We show the same U-Net can be used to both start the reversion and perform denoising diffusion afterwards, shortening the reverse diffusion chain by orders of magnitude while adding no more generator parameters and maintaining high generation quality.
- We show how to learn this implicit distribution in multiple different ways and ensure the robustness of the proposed TDPM.
- We show that TDPM can adjust its truncation level freely to strike a good balance between data generation quality and computational complexity.

## 2 Preliminaries on diffusion models

In Gaussian diffusion models (Sohl-Dickstein et al., 2015; Ho et al., 2020), starting from the data distribution  $\mathbf{x}_0 \sim q(\mathbf{x}_0)$ , a pre-defined forward diffusion process  $q_t$  produces auxiliary variables  $\mathbf{x}_{t=1:T}$  by gradually adding Gaussian noise, with variance  $\beta_t \in (0, 1)$  at time  $t$ , as follows:

$$q(\mathbf{x}_1, \dots, \mathbf{x}_T | \mathbf{x}_0) := \prod_{t=1}^T q(\mathbf{x}_t | \mathbf{x}_{t-1}), \quad q(\mathbf{x}_t | \mathbf{x}_{t-1}) := \mathcal{N}(\mathbf{x}_t; \sqrt{1 - \beta_t} \mathbf{x}_{t-1}, \beta_t \mathbf{I}). \quad (1)$$

With the limit of small diffusion rate, which means if  $\beta_t$  is scheduled to be sufficiently small, given  $q(\mathbf{x}_t | \mathbf{x}_{t-1})$  is Gaussian, the reverse distribution  $q(\mathbf{x}_{t-1} | \mathbf{x}_t)$  also follows a Gaussian

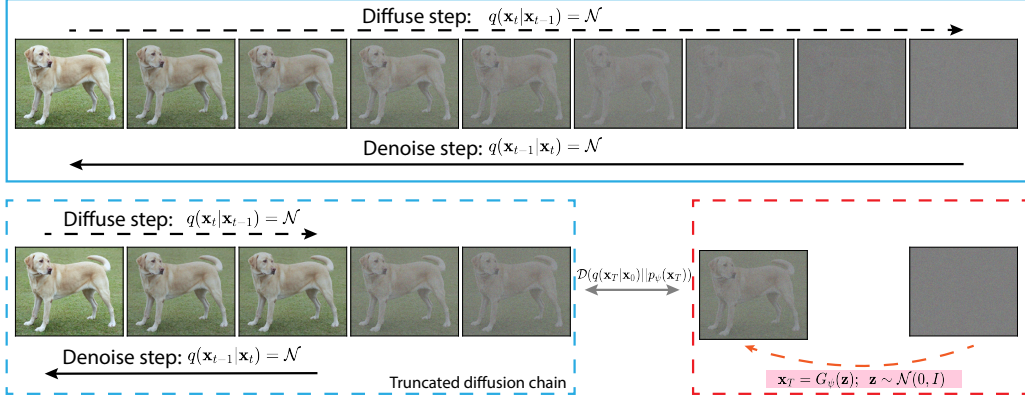


Figure 1: (Best viewed in color) An illustrative depiction of current diffusion models and our truncated diffusion models. **Top:** The conventional denoising diffusion models add Gaussian noise gradually with a large number of time steps, where the true denoising posterior can be kept close to Gaussian and hence easy to fit (marked in solid blue box). **Bottom:** Truncated diffusion models truncate the diffusion chain to keep its first few steps and small diffusion segment (marked in the dashed blue box). The truncated diffusion chain can be learned with conventional methods. Meanwhile, as the left part is truncated, the Gaussian prior  $p(\mathbf{x}_T)$  will have a large gap to  $q(\mathbf{x}_T | \mathbf{x}_0)$ , which is bridged with an implicit generative distribution (marked in dashed red box) that can be parameterized with the same U-Net used at the denoising steps.

distribution (Feller, 1949; Sohl-Dickstein et al., 2015) and can be approximated using a neural network parameterized Gaussian distribution  $p_\theta$  as:

$$p_\theta(\mathbf{x}_{t-1} | \mathbf{x}_t) := \mathcal{N}(\mathbf{x}_{t-1}; \mu_\theta(\mathbf{x}_t, t), \Sigma_\theta(\mathbf{x}_t, t)). \quad (2)$$

Moreover, with a sufficiently large  $T$ , the outcome of the diffusion chain  $\mathbf{x}_T$  will follow an isotropic Gaussian distribution. Thus, with the pre-defined forward (inference) diffusion process and the learned inverse (generative) diffusion process, we can sample from  $\mathbf{x}_T \sim \mathcal{N}(\mathbf{0}, \mathbf{I})$  and run the diffusion process in reverse to get a sample from the data distribution  $q(\mathbf{x}_0)$ .

Under the variational inference (Beal, 2003; Kingma & Welling, 2013; Blei et al., 2017) framework, viewing  $q(\mathbf{x}_1, \dots, \mathbf{x}_T | \mathbf{x}_0)$  in Equation 1 as the inference network, we can use the evidence lower bound (ELBO) as our learning objective. Following previous works Sohl-Dickstein et al. (2015); Ho et al. (2020), the ELBO of a diffusion probabilistic model can be expressed as

$$\mathcal{L}_{\text{ELBO}} := \mathcal{L}_0 + \sum_{t=2}^T \mathcal{L}_{t-1} + \mathcal{L}_T, \quad \mathcal{L}_0 := \mathbb{E}_q [-\log p_\theta(x_0 | x_1)], \quad (3)$$

$$\mathcal{L}_{t-1} := \mathbb{E}_q [D_{\text{KL}}(q(x_{t-1} | x_t, x_0) || p_\theta(x_{t-1} | x_t))], \quad (4)$$

$$\mathcal{L}_T := \mathbb{E}_q [D_{\text{KL}}(q(x_T | x_0) || p(x_T))], \quad (5)$$

where  $D_{\text{KL}}(q || p)$  denotes the Kullback–Leibler (KL) divergence from distributions  $p$  to  $q$ . Generally speaking, diffusion probabilistic models assume the number of diffusion steps  $T$  to be sufficiently large to satisfy two conditions: 1) the reverse distribution at each denoising step can be fitted with a Gaussian generator  $p_\theta(\mathbf{x}_{t-1} | \mathbf{x}_t)$ ; 2) with a sufficiently small diffusion rate  $\beta_t$ , the long forward diffusion process will successfully corrupt the data distribution such that  $\mathcal{L}_T$  will become close to zero, i.e.,  $q(x_T | x_0) \approx \mathcal{N}(\mathbf{0}, \mathbf{I})$ , and do not depend on  $\theta$ .

## What happens if $T$ is insufficiently large?

Recent works focus on reducing the number of diffusion steps from the order of thousands to fewer than ten (Xiao et al., 2021b). Given a data distribution  $q(\mathbf{x}_0)$  that is non-Gaussian, when the number of denoising steps are reduced, the true posterior  $q(\mathbf{x}_{t-1} | \mathbf{x}_t)$  is not a Gaussian distribution and usually intractable (Feller, 1949), which results in new challenges to current diffusion models.

As noted in Xiao et al. (2021b), when  $\beta_t$  is not sufficiently small, the diffusion step becomes larger and the denoising distribution can be multi-modal and hence too complex

to be well fit by Gaussian. The authors propose to define  $p_\theta(\mathbf{x}_{t-1} | \mathbf{x}_t)$  with a conditional generator and substitute the ELBO with

$$\min_{\theta} \sum_{t \geq 1} \mathbb{E}_{q(t)} [D_{\text{adv}}(q(\mathbf{x}_{t-1} | \mathbf{x}_t) \| p_\theta(\mathbf{x}_{t-1} | \mathbf{x}_t))], \quad (6)$$

where  $D_{\text{adv}}$  represents a statistical distance that relies on an adversarial training setup. This modified objective can be effectively minimized by leveraging the power of conditional GANs in fitting implicit multimodal distributions (Arjovsky et al., 2017; Goodfellow et al., 2014; Nowozin et al., 2016). While showing promising results, the proposed diffusion models in Xiao et al. (2021b) are shown to work the best when the number of diffusion steps is limited to be as small as four, and start to exhibit deteriorated performance when further increasing that number.

### 3 Method

In this section, we introduce TDPM that provides a new way to reduce the number of diffusion steps, without increasing the diffusion rate of the forward chain or substantially altering the ELBO.

#### 3.1 Truncated diffusion chains

Given a forward diffusion chain, whose length  $T$  is sufficiently large to map the data distribution into a Gaussian noise distribution, TDPM truncates the tail of this chain by only keeping the first  $\tilde{T}$  steps, where we choose  $\tilde{T} \ll T$  to substantially reduce the computational complexity in both training and generation. The consequence of this truncation is that while the diffusion rates  $\beta_t$  (and hence the forward chain) are kept the same for the first  $\tilde{T}$  steps, the forward chain becomes too short to map the data into a Gaussian random noise. As in Figure 1, in the truncated diffusion chain shown in the bottom row, the data are diffused into corrupted ones that have not yet completely become noise. As the diffusion rates have been kept small, this method allows the clean data to be well recovered by a few Gaussian denoising steps from the corrupted one. Compared to the original chain, this truncated one has a much shorter length and can be learned much more efficiently. A distinction from the original chain is that now the starting point of the inverse diffusion process becomes an unknown distribution, raising a new challenge in sampling. To tackle this challenge, we propose to use an implicit generative distribution to approximate the corrupted data distribution, by minimizing the difference between these two distributions.

Mathematically, recall that the ELBO in Equation 3 consists of three terms:  $\mathcal{L}_0$ ,  $\sum_{t=2}^T \mathcal{L}_{t-1}$ , and  $\mathcal{L}_T$ . The training objective of conventional diffusion models focus on terms  $\sum_{t=2}^T \mathcal{L}_{t-1}$  and  $\mathcal{L}_0$ . They assume  $\mathcal{L}_T$  does not depend on any parameter and it will be close to zero by carefully pre-define the forward noising process such that  $q(\mathbf{x}_T | \mathbf{x}_0) \approx p(\mathbf{x}_T) = \mathcal{N}(\mathbf{0}, \mathbf{I})$ . In the case where the chain is truncated, while we no longer have  $p(\mathbf{x}_T) = \mathcal{N}(\mathbf{0}, \mathbf{I})$ , we can reformulate it as an implicit distribution and infer its parameter by minimizing  $\mathcal{L}_T$  as:

$$\min_{\theta} \mathcal{L}_T = \min_{\theta} \mathcal{D}(q(\mathbf{x}_T | \mathbf{x}_0) \| p_\theta(\mathbf{x}_T)), \quad (7)$$

$$p_\theta(\mathbf{x}_T) = \int p(\mathbf{x}_T | \mathbf{z}) p(\mathbf{z}) d\mathbf{z}; \quad p(\mathbf{z}) = \mathcal{N}(\mathbf{0}, \mathbf{I}), \quad (8)$$

where  $\mathcal{D}(q \| p)$  denotes a statistical distance between distributions  $q$  and  $p$ , and  $p(\mathbf{z})$  is set as an isotropic Gaussian distribution to sample from.

#### 3.2 Fitting implicit distributions to bridge the gap

Our goal is to fit an implicit generative distribution  $p_\theta(\mathbf{x}_T)$  with the objective in Equation 7 to bridge the gap between the noise distribution and the corrupted data distribution. As  $p_\theta$  is implicit, we are not able to compare it with explicit density functions, but are allowed to take random samples from it. Therefore, we consider for  $\mathcal{D}(q(\mathbf{x}_T | \mathbf{x}_0) \| p_\theta(\mathbf{x}_T))$  two different types of statistical distances that can be estimated given random samples from both  $q$  and  $p$ . We find that the performance of TDPM is not sensitive to which statistical distance has been used for minimization.

Our first choice is to utilize GANs (Goodfellow et al., 2014; Arjovsky et al., 2017; Bińkowski et al., 2018), which are known as powerful tools to fit an implicit distribution. Suppose the

data dimension is  $d$ . Denoting  $D_\phi(\cdot) : \mathbb{R}^d \rightarrow [0, 1]$  as the discriminator and  $G_\theta(\cdot) : \mathbb{R}^d \rightarrow \mathbb{R}^d$  as the generator, the discriminator takes a sample  $\mathbf{x}_T$  as input and outputs the probability to determine whether it comes from the corrupted data distribution  $q(\mathbf{x}_T | \mathbf{x}_0)$  or from the implicit generative distribution  $p_\theta(\mathbf{x}_T)$ ; the generator takes a sample from the isotropic Gaussian  $p(\mathbf{z})$  and transforms it to approximate the corrupted data. The training objective  $\mathcal{L}_T^{\text{GAN}}$  is formulated as

$$\min_{\theta} \max_{\phi} \mathbb{E}_{\mathbf{x} \sim q(\mathbf{x}_T | \mathbf{x}_0)} [\log D_\phi(\mathbf{x})] + \mathbb{E}_{\mathbf{z} \sim p(\mathbf{z})} [\log(1 - D_\phi(G_\theta(\mathbf{z})))]. \quad (9)$$

Our second choice is to utilize conditional transport (Zheng & Zhou, 2021), a recently proposed statistical distance that strikes a good balance between capturing distribution modes and the generation of high-quality samples. Similar to the training of GANs, the objective  $\mathcal{L}_T^{\text{CT}}$  can be expressed as:

$$\min_{\theta, \eta} \max_{\phi} \mathbb{E}_{\mathbf{x} \sim q(\mathbf{x}_T | \mathbf{x}_0)} [\mathbb{E}_{G_\theta(\mathbf{z}) \sim \pi_\eta(G_\theta(\mathbf{z}) | \mathbf{x}_T)} c(\mathbf{x}_T, G_\theta(\mathbf{z}))] + \mathbb{E}_{\mathbf{z} \sim p(\mathbf{z})} [\mathbb{E}_{\mathbf{x} \sim \pi_\eta(\mathbf{x}_T | G_\theta(\mathbf{z}))} c(\mathbf{x}_T, G_\theta(\mathbf{z}))], \quad (10)$$

where  $\pi_\eta$  is a conditional distribution parameterized by  $\eta$  to find an optimal mapping between the samples of  $p$  and  $q$ .

### 3.3 Training objective

Given the fact that the objective in Equation 3 is a sum of independent terms  $\mathcal{L}_{t-1}$ , DDPM (Ho et al., 2020) simplifies this formulation and suggests to uniformly sample  $t$  for each image in each mini-batch by minimizing a simple noise prediction loss:

$$\mathcal{L}_{\text{simple}} = \mathbb{E}_{t, \mathbf{x}_0, \epsilon} [||\epsilon - \epsilon_\theta(\mathbf{x}_t, t)||^2]. \quad (11)$$

This objective is regarded as a simplified loss of  $\mathcal{L}_{\text{ELBO}}$  by fixing the terms  $\Sigma_\theta(x_t, t) = \sigma_t^2 \mathbf{I}$  and assuming  $\mathcal{L}_T$  to be zero with the pre-defined long forward diffusion chain. Here we put  $\mathcal{L}_T$  back to complete the variational objective in the truncated diffusion chain as:

$$\mathcal{L}_{\text{TDPM}}^{\text{GAN}} = \mathcal{L}_{\text{simple}} + \mathcal{L}_T^{\text{GAN}}, \quad (12)$$

$$\text{or} \quad \mathcal{L}_{\text{TDPM}}^{\text{CT}} = \mathcal{L}_{\text{simple}} + \mathcal{L}_T^{\text{CT}}. \quad (13)$$

While the weight of  $\mathcal{L}_T$  can be tuned, we fix it as one for simplicity. Here the TDPM objective consists of two parts: the denoising part  $\epsilon_\theta$  is focused on denoising the truncated chain, getting updated from  $\mathcal{L}_{\text{simple}}$ , while the implicit part  $G_\theta$  is focused on minimizing  $\mathcal{D}(q(\mathbf{x}_T | \mathbf{x}_0) || p_\theta(\mathbf{x}_T))$ , getting updated from either  $\mathcal{L}_T^{\text{GAN}}$  or  $\mathcal{L}_T^{\text{CT}}$ . We empirically find out Equations 12 and 13 have no significant difference in their final results as long as the generator is well trained. It is worth noting that the formulation of  $\mathcal{L}_T$  could also have several different parameterizations, which would result in versatile training strategies.

## 4 Experiments

As previously suggested, TDPM can obtain better sampling efficiency while ensuring the sample quality when the chain is truncated to a shorter length. We first validate our method with toy experiments on synthetic data, and then provide further empirical evidence on standard image datasets. For all experiments, we follow the same settings and architectures used in DDPM (Ho et al., 2020). The denoising generator has a U-Net structure (Ronneberger et al., 2015) using the Transformer sinusoidal position embedding (Vaswani et al., 2017) for diffusion step index. The implicit generator uses the same U-Net, without such embedding (or with the embedding but the step index is fixed at  $T + 1$ ). Under this setting, TDPM adds no extra parameters into the generator. The discriminator architecture is adopted from Karras et al. (2020b). Unless specified otherwise, the forward noise schedule is set by converting the linear schedule between  $\beta_1 = 10^{-4}$  and  $\beta_{1000} = 2 \times 10^{-2}$  in DDPM’s original setting, according to the desired number of steps  $T$  in TDPM with ratio  $\frac{T}{1000}$  i.e.,  $\beta_T = 2 \times 10^{-2} \times T/1000$ . More details regarding the experimental settings can be found in Appendix C. Note to compare to a DDPM with a diffusion chain of  $T$  steps, we will use a TDPM of  $T - 1$  steps, and hence both DDPM and TDPM will have the same Number of Function Evaluations (NFE) via the U-Net needed for generating an image.

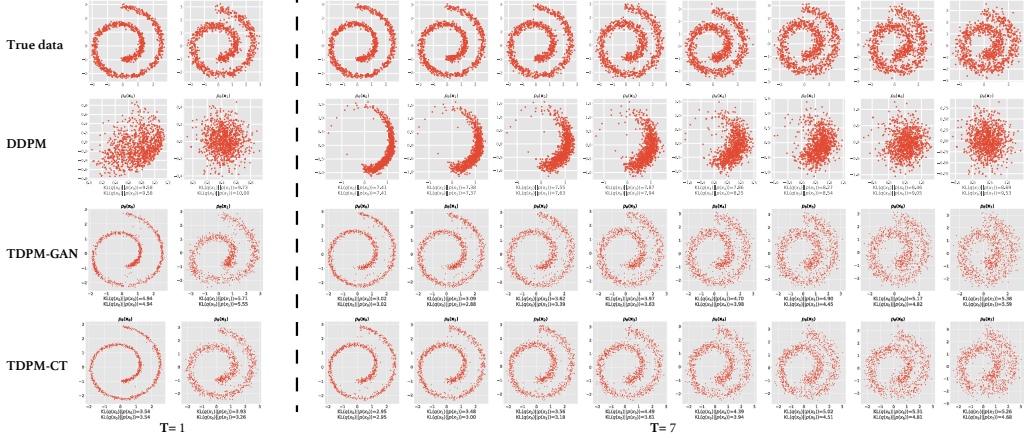


Figure 2: A comparison of DDPM (Ho et al., 2020), TDPM-GAN, and TDPM-CT on Swiss Roll toy data. We show the effects of a truncated diffusion chain with length  $T = 1$  (**Left**) and  $T = 7$  (**Right**). The first row displays the diffusion process from  $q(\mathbf{x}_0)$  to  $q(\mathbf{x}_T)$ . Each row below the first line represents the corresponding denoising distribution  $p_\theta(\mathbf{x}_{t-1} | \mathbf{x}_t)$ . DDPM assumes  $p(\mathbf{x}_T) = \mathcal{N}(\mathbf{0}, \mathbf{I})$  and we can observe a gap between the true data distribution and generative distribution, especially when the chain is shortened to  $T = 1$ . TDPM learns  $p_\theta(\mathbf{x}_T)$ , which can be observed to well approximate the true  $q(\mathbf{x}_T)$ . This helps the model successfully recover the clean data distribution  $q(\mathbf{x}_0)$  from the corrupted distribution  $q(\mathbf{x}_t | \mathbf{x}_0)$ . Below each model, we report empirical KL divergence between true data distributions and generative distributions as the quantitative metric. More results on different toy data can be found in Appendix A.

#### 4.1 Analysis on synthetic toy datasets

As a proof of concept, we first justify our method on representative 2D synthetic datasets used in prior works (Gulrajani et al., 2017; Zheng & Zhou, 2021), including Swiss Roll, Double Moons, 8-modal, and 25-modal Gaussian mixtures with equal component weights. We use an empirical sample set  $\mathcal{X}$ , consisting of  $|\mathcal{X}| = 2,000$  samples and illustrate the generated samples after 5000 training epochs. We take 20 grids in the range  $[-10, 10]$  for both the  $x$  and  $y$  axes to approximate the empirical distribution of  $\hat{p}_\theta$  and  $\hat{q}$ , and report the corresponding forward KL  $D_{\text{KL}}(\hat{q} || \hat{p}_\theta)$  as the quantitative evaluation metric.

Figure 2 shows the results on the Swiss Roll data. We present a short chain with  $T = 1$  and a longer chain with  $T = 7$  to show the impacts of the number of diffusion steps. The first row shows that the data distribution is diffused with accumulated noise, and with more steps the diffused distribution will be closer to an isotropic Gaussian distribution. As one can see, truncating the diffusion chain to a short length will result in a clear gap between  $p(\mathbf{x}_T)$  and  $\mathcal{N}(\mathbf{0}, \mathbf{I})$ . When DDPM (shown in the second row) samples from the isotropic Gaussian distribution, it becomes hard to recover the original data distribution from pure noise with only a few steps. Although we can see DDPM can get slightly improved with a few more steps ( $T = 8$ ), as long as  $p(\mathbf{x}_T)$  is not close to Gaussian, DDPM can hardly recover the data distribution. By contrast, as shown in the third and fourth rows, TDPM successfully approximates the non-Gaussian  $q(\mathbf{x}_T)$  with its implicit generator, and we can see the remaining part of the truncated chain is gradually recovered by the denoising steps. From both visualizations and  $D_{\text{KL}}(\hat{q} || \hat{p}_\theta)$ , we can see that TDPM is able to fit every step in such short chains.

By comparing TDPM-GAN and TDPM-CT, we can find the latter one fits  $p_\theta(\mathbf{x}_T)$  slightly better, *e.g.* when  $T = 2$ , we have the empirical KL 5.71 of TDPM-GAN *vs.* 3.93 of TDPM-CT. As a result, the KL in the data step has 4.94 *vs.* 3.54. This observation confirms the importance of fitting the implicit generative distribution. If we have a perfect implicit generator to model  $p(\mathbf{x}_T)$ , then the number of steps in need can be compressed to a small number. On the contrary, if the implicit generator is not sufficiently powerful, we need more steps to facilitate the fitting of the data distribution. We have also compared TDPM-GAN with TDPM-CT on natural images and found TDPM-GAN in general performs better. For simplicity, unless specified otherwise, in what follows TDPM by default represents the TDPM-GAN setting.

Table 1: Results of unconditional generation on CIFAR-10. Models are grouped by the orders of sampling steps, with the best IS, FID, and Recall in each group marked in bold.

Model	NFE ↓	IS↑	FID↓	Recall ↑
Improved DDPM (Nichol & Dhariwal, 2021)	4000	-	2.90	-
UDM (Kim et al., 2021)	2000	<b>10.1</b>	2.33	-
Likelihood SDE (Song et al., 2021a)	2000	-	2.87	-
Score SDE (VE) (Song et al., 2021b)	2000	9.89	<b>2.20</b>	0.59
Score SDE (VP) (Song et al., 2021b)	2000	9.68	2.41	0.59
NCNN (Song & Ermon, 2019)	1000	8.87	25.3	-
Adversarial DSM (Jolicoeur-Martineau et al., 2020)	1000	-	6.10	-
VDM (Kingma et al., 2021)	1000	-	4.00	-
D3PMs (Austin et al., 2021)	1000	8.56	7.34	-
DiffuseVAE (Pandey et al., 2022), T=1000	1000	8.63	8.72	-
DDPM (Ho et al., 2020)	1000	<b>9.46</b>	3.21	0.57
TDPM, T=999 (ours)	1000	9.24	<b>3.07</b>	0.57
Recovery EBM (Gao et al., 2021)	180	8.30	9.58	-
Gotta Go Fast (Jolicoeur-Martineau et al., 2021)	180	-	2.44	-
LSGM (Vahdat et al., 2021)	147	<b>9.87</b>	<b>2.10</b>	<b>0.61</b>
Probability Flow (VP) (Song et al., 2021b)	140	9.83	3.08	0.57
DiffuseVAE (Pandey et al., 2022), T=100	100	8.27	11.71	-
TDPM, T=99 (ours)	100	9.34	3.10	0.57
FastDDPM, T=50 (Kong & Ping, 2021)	50	8.98	3.41	0.56
DDIM, T=50 (Song et al., 2020)	50	8.78	4.67	0.53
SNGAN+DGflow (Ansari et al., 2021)	25	<b>9.35</b>	9.62	0.48
TDPM, T=49 (ours)	50	9.22	<b>3.30</b>	<b>0.57</b>
DDPM Distillation (Luhman & Luhman, 2021)	1	8.36	9.36	<b>0.51</b>
SNGAN (Miyato et al., 2018)	1	8.22	21.7	0.44
AutoGAN (Gong et al., 2019)	1	8.60	12.4	0.46
TransGAN (Jiang et al., 2021)	1	9.02	9.26	-
StyleGAN2 w/o ADA (Karras et al., 2020a)	1	9.18	8.32	0.41
StyleGAN2 w/ ADA (Karras et al., 2020a)	1	<b>9.83</b>	<b>2.92</b>	0.46
StyleGAN2 w/ DiffAug (Zhao et al., 2020)	1	9.40	5.79	0.42
Denoising Diffusion GAN (Xiao et al., 2021b), T=1	1	8.93	14.6	0.19
TDPM, T=0 (ours)	1	8.65	8.91	0.46
Denoising Diffusion GAN (Xiao et al., 2021b), T=2	2	<b>9.80</b>	4.08	0.54
Denoising Diffusion GAN (Xiao et al., 2021b), T=4	4	9.63	3.75	<b>0.57</b>
Denoising Diffusion GAN (Xiao et al., 2021b), T=8	8	9.43	4.36	0.56
TDPM, T=1 (ours)	2	8.97	4.47	0.53
TDPM, T=3 (ours)	4	9.00	<b>3.41</b>	<b>0.57</b>

## 4.2 Comparing with SoTAs on image datasets

In this section, following the convention, we compare TDPM with the state of the arts (SoTAs) on natural image datasets, including CIFAR-10 (Krizhevsky et al., 2009), CelebA, CelebA-HQ (Liu et al., 2015), LSUN bedroom, and LSUN Church (Yu et al., 2015). The resolutions of inputs are set as  $32 \times 32$  for CIFAR-10,  $64 \times 64$  for CelebA, and  $256 \times 256$  for CelebA-HQ, LSUN bedroom, and LSUN Church. For evaluation metric, we adopt the commonly used Fréchet inception distance (FID, lower is preferred) (Heusel et al., 2017), Inception Score (IS, higher is preferred), and Recall (a generation diversity measure (Kynkäanniemi et al., 2019), higher is preferred). We keep the same training setting as DDPM (Ho et al., 2020), and run experiments by setting NFE = 4, 50, 100, and 1000 ( $T = \text{NFE}$  for DDPM and  $T = \text{NFE} - 1$  for TDPM). Notably, a key difference between TDPM and DDPM is whether  $p(\mathbf{x}_T)$  is trained to be close to  $q(\mathbf{x}_T | \mathbf{x}_0)$ .

**Main results:** We first compare with representative deep generative models (DGMs) on CIFAR-10, a widely used benchmark. We report the results in Table 1, where we follow Xiao et al. (2021b) to group the models according to their NFE, which equals to the number of U-Net based sampling steps for diffusion models. We observe that our TDPM in general improves the sample quality and efficiency. Notably, when NFE = 1000, although keeping the same setting as DDPM, encouraging  $p_\theta(\mathbf{x}_T)$  to approach  $q(\mathbf{x}_T | \mathbf{x}_0)$  brings positive effects to improve FID. Moreover, we observe TDPM still achieves good FID and Inception score even when its NFE =  $T + 1$  is reduced to be as small as 4, where the denoising process is largely reduced compared to DDPM and conventional diffusion models. Based on the observations in Table 1, truncating the diffusion chain to a short length results in a slight drop in performance in terms of FID, while there is no indication that the generation diversity is lowered, which suggests the implicit model does not suffer mode dropping problems like GANs. Comparing with all SoTA DGMs, the sample quality of TDPM is competitive, as we can see TDPM reaches the best FID in the group with NFE = 50 and 1000.

**On the effects of diffusion steps:** In this part, we investigate the trade-off between performance and computation cost in TDPM. We compare the performance of TDPM across  $T=0$  (without diffusion), and  $T \in \{1, 3, 49, 99, 999\}$  on CIFAR-10. We report both FID and



Figure 3: Qualitative visualizations on CIFAR-10 and CelebA ( $64 \times 64$ ), produced by TDPM-GAN and TDPM-CT ( $T = 3$ ).

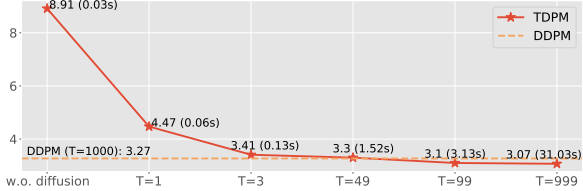


Figure 4: Evolution of FID and corresponding GPU time (s/image) in the sampling *v.s.* diffusion timesteps. The orange dashed line marks the performance of DDPM with  $T = 1000$ .

Table 2: Results on CelebA ( $64 \times 64$ ).

Model	NFE	FID $\downarrow$
COCO-GAN (Lin et al., 2019)	1	4.00
QA-GAN (Parimala & Channappayya, 2019)	1	6.42
VAE-BM (Xiao et al., 2021a)	1	5.31
NVAE (Vahdat & Kautz, 2020)	1	14.74
DiffuseVAE (Pandey et al., 2022)	1000	4.76
DDPM (Ho et al., 2020)	1000	5.98
TDPM, T=99	100	3.14
TDPM, T=49	50	3.28
TDPM, T=3	4	3.96

the sampling time (s/image) on one V100 GPU in Figure 4. Without diffusion, TDPM is equivalent to a GAN whose generator is a U-Net, and we can see clearly the performance gap compared with the results of  $T > 0$ . Comparing results across  $T$ , the FID of  $T = 3$  is significantly lower than FID of  $T = 1$ , while the computation time slightly increases. Further increasing  $T$  leads to a further reduction of FID, though at a much slower reduction rate as  $T$  becomes larger. This reduction comes with the expense of linearly increasing the generation time that is proportional to  $\text{NFE} = T + 1$ . When  $T = 99$ , the FID of TDPM becomes better than DDPM with  $T = 1000$ . Given the slow reduction in FID as  $T$  increases, a small  $T$  equal to or larger than 3 is recommended to have a good compromise between the generation quality and speed.

**Results on higher solution images:** We also validate TDPM on higher-resolution images. Here we mainly use DDPM as a baseline and compare it with TDPM across different  $T$ . This aims to verify whether using truncated chains in TDPM also improves the efficiency of diffusion models on more complex data. We train TDPM on CelebA at  $64 \times 64$  and on LSUN Church/Bedroom (Yu et al., 2015) at  $256 \times 256$  resolution. The FIDs are reported in Tables 2, 3, and 4. We include the FIDs of representative GANs, VAEs, and DDPM as references. Note the most relevant comparison is between DDPM and TDPM as they share the exactly same U-Net for data generation; the other models are mainly included as references due to the differences in model sizes and architectures. The results show that TDPM has competitive generation performance, and consistently improves DDPM in terms of FID, under significantly smaller  $T$  and hence substantially faster generation.

**Qualitative visualization:** We show qualitative results in Figures 3, 5, and 6 as visual justifications of our enhanced quantitative results in Tables 1, 2, 3, and 4. Notably, in Figures 5 and 6, we show the samples from the implicit generative distribution  $\mathbf{x}_T \sim p_\theta(\mathbf{x}_T)$  and their corresponding  $\mathbf{x}_0$ . As the length of chain is truncated shorter, we can observe  $\mathbf{x}_T$  is required to be more similar to the clean sample  $\mathbf{x}_0$ , which confirms our analysis in toy experiments: the same U-Net used for denoising can simultaneously serve as a powerful implicit generator, allowing the chain to be truncated to have only a few steps; otherwise, more diffusion steps are in need if the corrupted data remain hard to approximate by the U-Net based generator.

## 5 Related work

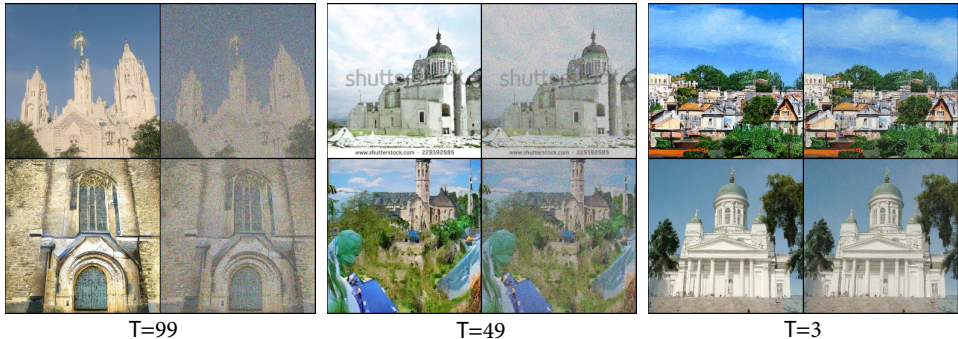
Diffusion probabilistic models (Sohl-Dickstein et al., 2015; Ho et al., 2020) employ a forward Markov chain to diffuse the data to noise and learn the reversal of such a diffusion process.

Table 3: Results on LSUN Church (256 × 256).

Model	NFE	FID $\downarrow$
Gotta Go Fast (Jolicoeur-Martineau et al., 2021)	270	25.67
Denoising Diffusion GAN (Xiao et al., 2021b)	4	5.25
StyleGAN2 (Karras et al., 2020b)	1	3.93
CIPS (Anokhin et al., 2021)	1	2.92
DDPM (Ho et al., 2020)	1000	7.89
TDPM, T=99	100	4.33
TDPM, T=49	50	5.35
TDPM, T=3	4	5.02

Table 4: Results on LSUN Bedroom (256 × 256).

Model	NFE	FID $\downarrow$
UDM (Kim et al., 2021)	2000	4.57
ADM (Dhariwal & Nichol, 2021)	1000	1.90
PGGAN (Karras et al., 2018)	1	8.34
StyleGAN2 (Karras et al., 2020b)	1	3.98
DDPM (Ho et al., 2020)	1000	4.90
TDPM, T=99	100	3.95
TDPM, T=49	50	4.10
TDPM, T=3	4	4.21

Figure 5: Qualitative results of TDPM on LSUN Church (256 × 256), with  $T = 99$ ,  $T = 49$ , and  $T = 3$ . Note NFE =  $T + 1$  in TDPM. Each group presents the generated samples from  $p_\theta(\mathbf{x}_0)$  (left) and  $p_\theta(\mathbf{x}_T)$  (right).

With the idea of exploiting the Markov operations (Goyal et al., 2017; Alain et al., 2016; Bordes et al., 2017), diffusion models achieve great success and inspire a variety of tasks including image generation and audio generation (Kong et al., 2020; Chen et al., 2020; Jolicoeur-Martineau et al., 2020; Vahdat et al., 2021). Recently, plenty of studies have been proposed to generalize diffusion model to continuous time diffusion and improve the diffusion models in likelihood estimation (Vincent, 2011; Song & Ermon, 2020, 2019; Nichol & Dhariwal, 2021; Song et al., 2021b,a; Kingma et al., 2021).

Another mainstream is to improve the sampling efficiency of diffusion models, which are known for their enormous number of sampling steps. Luhman & Luhman (2021) improve diffusion processes with knowledge distillation and San-Roman et al. (2021) propose a learnable adaptive noise schedule. Song et al. (2020) and Kong & Ping (2021) exploit non-Markovian diffusion processes and shorten the denoising segments. Jolicoeur-Martineau et al. (2021) and Huang et al. (2021) use better SDE solvers for continuous-time models. Aside from these works, recently other types of generative models such as VAEs (Kingma & Welling, 2013), GANs (Goodfellow et al., 2014), and autoregressive models (Van den Oord et al., 2016) have been incorporated to diffusion models. They are shown to benefit each other (Xiao et al., 2021b; Pandey et al., 2022; Meng et al., 2021) and have closer relation to our work. Xiao et al. (2021b) consider the use of implicit models (Huszár, 2017; Mohamed & Lakshminarayanan, 2016; Tran et al., 2017; Yin & Zhou, 2018; Li & Malik, 2018) to boost the efficiency of diffusion models, where they deploy implicit models in each denoising step, which has higher difficulty in the training as the number of diffusion steps increases. Pandey et al. (2022) build diffusion models on top of the output of VAEs for refinement. Our work is also related if viewing TDPM as a diffusion model on top of an implicit model, where the implicit model has better flexibility and produces samples with higher fidelity. A key distinction is that TDPM makes the same U-Net not only perform denoising but also parameterize the implicit model, adding no extra parameters into the data generation process.

## 6 Conclusion

In this paper, we investigate how to reduce the trajectory length of the diffusion chain to achieve efficient sampling without loss of generation quality. We propose truncated diffusion probabilistic modeling (TDPM) that truncates the length of a diffusion chain. In this way, TDPM can use a much shorter diffusion chain, while being required to start the reverse denoising process from an intractable distribution. We propose to learn such a distribution with an implicit generative model powered by the same U-Net used for denoising diffusion, and validate with multiple ways to learn the implicit distribution to ensure the robustness of



Figure 6: Analogous qualitative results to Figure 5 on LSUN Bedroom. Produced by TDPM.

the proposed TDPM. We conduct extensive experiments on both synthetic and real image data to demonstrate the effectiveness of TDPM in terms of both sample quality and efficiency, where the diffusion chain can be shortened to have only a few steps.

## References

Alain, G., Bengio, Y., Yao, L., Yosinski, J., Thibodeau-Laufer, E., Zhang, S., and Vincent, P. Gsns: generative stochastic networks. *Information and Inference: A Journal of the IMA*, 5(2):210–249, 2016.

Anokhin, I., Demochkin, K., Khakhulin, T., Sterkin, G., Lempitsky, V., and Korzhenkov, D. Image generators with conditionally-independent pixel synthesis. In *Proceedings of the IEEE/CVF Conference on Computer Vision and Pattern Recognition (CVPR)*, pp. 14278–14287, June 2021.

Ansari, A. F., Ang, M. L., and Soh, H. Refining deep generative models via discriminator gradient flow. In *International Conference on Learning Representations*, 2021.

Arjovsky, M., Chintala, S., and Bottou, L. Wasserstein generative adversarial networks. In *Proceedings of the 34th International Conference on Machine Learning-Volume 70*, pp. 214–223, 2017.

Austin, J., Johnson, D., Ho, J., Tarlow, D., and Berg, R. v. d. Structured denoising diffusion models in discrete state-spaces. *arXiv preprint arXiv:2107.03006*, 2021.

Beal, M. J. *Variational Algorithms for Approximate Bayesian Inference*. PhD thesis, UCL, 2003.

Bińkowski, M., Sutherland, D. J., Arbel, M., and Gretton, A. Demystifying MMD GANs. In *International Conference on Learning Representations*, 2018. URL <https://openreview.net/forum?id=r11U0zWCW>.

Blei, D. M., Kucukelbir, A., and McAuliffe, J. D. Variational inference: A review for statisticians. *Journal of the American statistical Association*, 112(518):859–877, 2017.

Bordes, F., Honari, S., and Vincent, P. Learning to generate samples from noise through infusion training. *arXiv preprint arXiv:1703.06975*, 2017.

Brock, A., Donahue, J., and Simonyan, K. Large scale GAN training for high fidelity natural image synthesis. In *International Conference on Learning Representations*, 2019. URL <https://openreview.net/forum?id=B1xsqj09Fm>.

Chen, N., Zhang, Y., Zen, H., Weiss, R. J., Norouzi, M., and Chan, W. Wavegrad: Estimating gradients for waveform generation, 2020.

Dhariwal, P. and Nichol, A. Q. Diffusion models beat GANs on image synthesis. In Beygelzimer, A., Dauphin, Y., Liang, P., and Vaughan, J. W. (eds.), *Advances in Neural Information Processing Systems*, 2021. URL <https://openreview.net/forum?id=AAWuCvzaVt>.

Feller, W. On the theory of stochastic processes, with particular reference to applications. In *Proceedings of the [First] Berkeley Symposium on Mathematical Statistics and Probability*, pp. 403–432. University of California Press, 1949.

Gao, R., Song, Y., Poole, B., Wu, Y. N., and Kingma, D. P. Learning energy-based models by diffusion recovery likelihood. In *International Conference on Learning Representations*, 2021.

Gong, X., Chang, S., Jiang, Y., and Wang, Z. Autogan: Neural architecture search for generative adversarial networks. In *Proceedings of the IEEE conference on computer vision and pattern recognition*, 2019.

Goodfellow, I., Pouget-Abadie, J., Mirza, M., Xu, B., Warde-Farley, D., Ozair, S., Courville, A., and Bengio, Y. Generative adversarial nets. In *Advances in Neural Information Processing Systems*, pp. 2672–2680, 2014.

Goyal, A., Ke, N. R., Ganguli, S., and Bengio, Y. Variational walkback: Learning a transition operator as a stochastic recurrent net. *arXiv preprint arXiv:1711.02282*, 2017.

Gulrajani, I., Ahmed, F., Arjovsky, M., Dumoulin, V., and Courville, A. C. Improved training of Wasserstein GANs. In *Advances in Neural Information Processing Systems*, pp. 5767–5777, 2017.

He, K., Zhang, X., Ren, S., and Sun, J. Deep residual learning for image recognition. In *Proceedings of the IEEE conference on computer vision and pattern recognition*, pp. 770–778, 2016.

Heusel, M., Ramsauer, H., Unterthiner, T., Nessler, B., and Hochreiter, S. GANs trained by a two time-scale update rule converge to a local Nash equilibrium. In *Advances in Neural Information Processing Systems*, pp. 6626–6637, 2017.

Ho, J., Jain, A., and Abbeel, P. Denoising diffusion probabilistic models. In *Advances in Neural Information Processing Systems*, 2020.

Huang, C.-W., Lim, J. H., and Courville, A. A variational perspective on diffusion-based generative models and score matching. *arXiv preprint arXiv:2106.02808*, 2021.

Huszár, F. Variational inference using implicit distributions. *arXiv preprint arXiv:1702.08235*, 2017.

Hyvärinen, A. and Dayan, P. Estimation of non-normalized statistical models by score matching. *Journal of Machine Learning Research*, 6(4), 2005.

Jiang, Y., Chang, S., and Wang, Z. Transgan: Two transformers can make one strong gan. *arXiv preprint arXiv:2102.07074*, 2021.

Jolicoeur-Martineau, A., Piché-Taillefer, R., des Combes, R. T., and Mitliagkas, I. Adversarial score matching and improved sampling for image generation, 2020.

Jolicoeur-Martineau, A., Li, K., Piché-Taillefer, R., Kachman, T., and Mitliagkas, I. Gotta go fast when generating data with score-based models. *arXiv preprint arXiv:2105.14080*, 2021.

Karras, T., Aila, T., Laine, S., and Lehtinen, J. Progressive growing of GANs for improved quality, stability, and variation. In *International Conference on Learning Representations*, 2018.

Karras, T., Laine, S., and Aila, T. A style-based generator architecture for generative adversarial networks. In *Proceedings of the IEEE/CVF Conference on Computer Vision and Pattern Recognition*, pp. 4401–4410, 2019.

Karras, T., Aittala, M., Hellsten, J., Laine, S., Lehtinen, J., and Aila, T. Training generative adversarial networks with limited data. *arXiv preprint arXiv:2006.06676*, 2020a.

Karras, T., Laine, S., Aittala, M., Hellsten, J., Lehtinen, J., and Aila, T. Analyzing and improving the image quality of stylegan. In *Proceedings of the IEEE conference on computer vision and pattern recognition*, 2020b.

Kim, D., Shin, S., Song, K., Kang, W., and Moon, I.-C. Score matching model for unbounded data score. *arXiv preprint arXiv:2106.05527*, 2021.

Kingma, D. P. and Ba, J. Adam: A method for stochastic optimization. In Bengio, Y. and LeCun, Y. (eds.), *3rd International Conference on Learning Representations, ICLR 2015, San Diego, CA, USA, May 7-9, 2015, Conference Track Proceedings*, 2015. URL <http://arxiv.org/abs/1412.6980>.

Kingma, D. P. and Welling, M. Auto-encoding variational Bayes. *arXiv preprint arXiv:1312.6114*, 2013.

Kingma, D. P., Salimans, T., Poole, B., and Ho, J. Variational diffusion models. *arXiv preprint arXiv:2107.00630*, 2021.

Kong, Z. and Ping, W. On fast sampling of diffusion probabilistic models. *arXiv preprint arXiv:2106.00132*, 2021.

Kong, Z., Ping, W., Huang, J., Zhao, K., and Catanzaro, B. Diffwave: A versatile diffusion model for audio synthesis, 2020.

Krizhevsky, A. et al. Learning multiple layers of features from tiny images. 2009.

Kynkänniemi, T., Karras, T., Laine, S., Lehtinen, J., and Aila, T. Improved precision and recall metric for assessing generative models. *Advances in Neural Information Processing Systems*, 32, 2019.

Li, K. and Malik, J. Implicit maximum likelihood estimation. *arXiv preprint arXiv:1809.09087*, 2018.

Lin, C. H., Chang, C.-C., Chen, Y.-S., Juan, D.-C., Wei, W., and Chen, H.-T. Coco-gan: Generation by parts via conditional coordinating. In *Proceedings of the IEEE/CVF International Conference on Computer Vision*, pp. 4512–4521, 2019.

Liu, Z., Luo, P., Wang, X., and Tang, X. Deep learning face attributes in the wild. In *Proceedings of the IEEE international conference on computer vision*, pp. 3730–3738, 2015.

Luhman, E. and Luhman, T. Knowledge distillation in iterative generative models for improved sampling speed. *arXiv preprint arXiv:2101.02388*, 2021.

Meng, C., Song, J., Song, Y., Zhao, S., and Ermon, S. Improved autoregressive modeling with distribution smoothing. *arXiv preprint arXiv:2103.15089*, 2021.

Miyato, T., Kataoka, T., Koyama, M., and Yoshida, Y. Spectral normalization for generative adversarial networks. In *International Conference on Learning Representations*, 2018.

Mohamed, S. and Lakshminarayanan, B. Learning in implicit generative models. *arXiv preprint arXiv:1610.03483*, 2016.

Neal, R. M. MCMC using Hamiltonian dynamics. *Handbook of Markov Chain Monte Carlo*, pp. 113, 2011.

Nichol, A. and Dhariwal, P. Improved denoising diffusion probabilistic models. *arXiv preprint arXiv:2102.09672*, 2021.

Nowozin, S., Cseke, B., and Tomioka, R. f-gan: Training generative neural samplers using variational divergence minimization. In *Advances in neural information processing systems*, 2016.

Pandey, K., Mukherjee, A., Rai, P., and Kumar, A. Diffusevae: Efficient, controllable and high-fidelity generation from low-dimensional latents. *arXiv preprint arXiv:2201.00308*, 2022.

Parimala, K. and Channappayya, S. Quality aware generative adversarial networks. *Advances in neural information processing systems*, 32:2948–2958, 2019.

Radford, A., Metz, L., and Chintala, S. Unsupervised representation learning with deep convolutional generative adversarial networks. *arXiv preprint arXiv:1511.06434*, 2015.

Razavi, A., Van den Oord, A., and Vinyals, O. Generating diverse high-fidelity images with VQ-VAE-2. *Advances in neural information processing systems*, 32, 2019.

Rezende, D. J., Mohamed, S., and Wierstra, D. Stochastic backpropagation and approximate inference in deep generative models. In *International conference on machine learning*, pp. 1278–1286. PMLR, 2014.

Ronneberger, O., Fischer, P., and Brox, T. U-net: Convolutional networks for biomedical image segmentation. In *International Conference on Medical image computing and computer-assisted intervention*. Springer, 2015.

San-Roman, R., Nachmani, E., and Wolf, L. Noise estimation for generative diffusion models. *arXiv preprint arXiv:2104.02600*, 2021.

Sohl-Dickstein, J., Weiss, E. A., Maheswaranathan, N., and Ganguli, S. Deep unsupervised learning using nonequilibrium thermodynamics, 2015.

Song, J., Meng, C., and Ermon, S. Denoising diffusion implicit models, 2020.

Song, Y. and Ermon, S. Generative modeling by estimating gradients of the data distribution. In *Advances in Neural Information Processing Systems*, pp. 11918–11930, 2019.

Song, Y. and Ermon, S. Improved techniques for training score-based generative models. *arXiv preprint arXiv:2006.09011*, 2020.

Song, Y., Durkan, C., Murray, I., and Ermon, S. Maximum likelihood training of score-based diffusion models. *arXiv e-prints*, pp. arXiv–2101, 2021a.

Song, Y., Sohl-Dickstein, J., Kingma, D. P., Kumar, A., Ermon, S., and Poole, B. Score-based generative modeling through stochastic differential equations. In *International Conference on Learning Representations*, 2021b. URL <https://openreview.net/forum?id=PxTIG12RRHS>.

Tran, D., Ranganath, R., and Blei, D. Hierarchical implicit models and likelihood-free variational inference. In *Advances in Neural Information Processing Systems*, pp. 5523–5533, 2017.

Vahdat, A. and Kautz, J. NVAE: A deep hierarchical variational autoencoder. In *Advances in neural information processing systems*, 2020.

Vahdat, A., Kreis, K., and Kautz, J. Score-based generative modeling in latent space. In *Advances in neural information processing systems*, 2021.

Van den Oord, A., Kalchbrenner, N., Espeholt, L., Vinyals, O., and Graves, A. Conditional image generation with PixelCNN decoders. *Advances in neural information processing systems*, 29, 2016.

Van Den Oord, A., Vinyals, O., et al. Neural discrete representation learning. *Advances in neural information processing systems*, 30, 2017.

Vaswani, A., Shazeer, N., Parmar, N., Uszkoreit, J., Jones, L., Gomez, A. N., Kaiser, L., and Polosukhin, I. Attention is all you need. In *Advances in neural information processing systems*, pp. 5998–6008, 2017.

Vincent, P. A connection between score matching and denoising autoencoders. *Neural computation*, 23(7):1661–1674, 2011.

Welling, M. and Teh, Y. W. Bayesian learning via stochastic gradient Langevin dynamics. In *Proceedings of the 28th international conference on machine learning (ICML-11)*, pp. 681–688. Citeseer, 2011.

Xiao, Z., Kreis, K., Kautz, J., and Vahdat, A. Vaebm: A symbiosis between variational autoencoders and energy-based models. In *International Conference on Learning Representations*, 2021a.

Xiao, Z., Kreis, K., and Vahdat, A. Tackling the generative learning trilemma with denoising diffusion gans. *arXiv preprint arXiv:2112.07804*, 2021b.

Yin, M. and Zhou, M. Semi-implicit variational inference. In *International Conference on Machine Learning*, pp. 5660–5669, 2018.

Yu, F., Seff, A., Zhang, Y., Song, S., Funkhouser, T., and Xiao, J. LSUN: Construction of a large-scale image dataset using deep learning with humans in the loop. *arXiv preprint arXiv:1506.03365*, 2015.

Zhao, S., Liu, Z., Lin, J., Zhu, J.-Y., and Han, S. Differentiable augmentation for data-efficient GAN training. *arXiv preprint arXiv:2006.10738*, 2020.

Zheng, H. and Zhou, M. Exploiting chain rule and Bayes' theorem to compare probability distributions. *Advances in Neural Information Processing Systems*, 34, 2021.

## A Additional Results

Below we provide complementary experimental results.

### A.1 Results of separately trained implicit generative models

As shown in Section 3, in general the objective of TDPM consists of the diffusion model objective (simple loss of DDPM  $\mathcal{L}_{\text{simple}}$ ) and an implicit model training objective  $\mathcal{L}_T^{\text{GAN}}$  or  $\mathcal{L}_T^{\text{CT}}$ . Without loss of generality, in our main paper, the implicit objective is jointly trained with the diffusion model loss, and the implicit part for  $t = T$  shares the same U-Net architecture used for  $0 < t < T$ . In this part, we investigate two cases:

- In the training of TDPM, we deploy different architecture to accomplish the fitting of the implicit distribution at  $t = T$  to validate the compatibility of TDPM with other architecture.
- The implicit part is separately trained with GAN objective. Specifically, we only train a GAN to fit the truncated endpoint of the diffusion train, and combine it with a pre-trained DDPM as a strategy to speed-up the sampling.

**Ablations of architecture of  $\theta_T$ :** In our main experiments, the implicit generator at step  $t = T$  shares the same U-Net architecture with  $t < T$ . Here we conduct the experiments by using Stylegan2 generator architecture Karras et al. (2020b) for  $\theta$  at  $t = T$ . The results on CIFAR-10, LSUN-bedroom, and LSUN-church are shown in Table 5. In this case, although the total parameter size of the generator also increases, as we need to specifically handle the training at  $t = T$ , we can see the FID results are consistently improved. The results here suggest that TDPM is not limited to a specific generator architecture and is able to incorporate different ways in fitting the implicit distribution at  $t = T$ .

Table 5: Results by training the implicit generator with Stylegan2 architecture. The FID gains compared with the results in Tables 1, 3, and 4 are noted in green, right next to the FID number.

Dataset	Parameter increase	Steps	FID $\downarrow$
CIFAR-10	+19M	T=99	2.88 <sub>-0.22</sub>
		T=49	2.94 <sub>-0.36</sub>
		T=3	3.19 <sub>-0.22</sub>
LSUN-bedroom	+28M	T=99	3.67 <sub>-0.28</sub>
		T=49	3.98 <sub>-0.12</sub>
		T=3	4.09 <sub>-0.12</sub>
LSUN-church	+28M	T=99	3.38 <sub>-0.95</sub>
		T=49	4.34 <sub>-0.99</sub>
		T=3	4.89 <sub>-0.13</sub>

**Separately train the implicit generator:** Different than the general settings, here we separately and only train the implicit model at  $t = T$ , and combine it with a pre-trained DDPM model<sup>1</sup> in the sampling phase. In training, as we only need to train the implicit model for  $t = T$ , the training time is largely reduced by about 8 hours with 8 V100 GPUs on CIFAR-10. In the sampling, shown in Table 6, when combined with a pre-trained DDPM for  $t < T$ , the generation is still compelling compared with those trained end-to-end.

### A.2 Additional results for toy experiments

In Section 4.1, we have validated our method with the Swiss Roll dataset. Here we show additional results on 8-modal Gaussian, 25-modal Gaussian, and Double-Moons data, shown in Figure 7-Figure 9. We can see 8-modal Gaussian is more similar to an isotropic Gaussian after getting diffused, thus DDPM can recover it even with 7 steps. On Double-Moons, we can observe with  $T = 1$ ,  $q(\mathbf{x}_T | \mathbf{x}_0)$  is not easy to approximate, while increasing  $T$  to 7 facilitates the learning of the generator. These observations confirm our analysis in Section 4.1.

<sup>1</sup>The pre-trained checkpoints are provided by: [https://github.com/pesser/pytorch\\_diffusion](https://github.com/pesser/pytorch_diffusion)

Table 6: Results by separately training the implicit generator on CIFAR-10.

Model ( $t = T$ )	Model ( $t < T$ )	Steps	FID $\downarrow$
TDPM (T=99)	TDPM	T=99	3.10
TDPM (T=99)	pre-trained DDPM	T=99	3.34
TDPM (T=49)	TDPM	T=49	3.30
TDPM (T=49)	pre-trained DDPM	T=49	3.55
TDPM (T=3)	TDPM	T=3	3.41
TDPM (T=3)	pre-trained DDPM	T=3	4.09

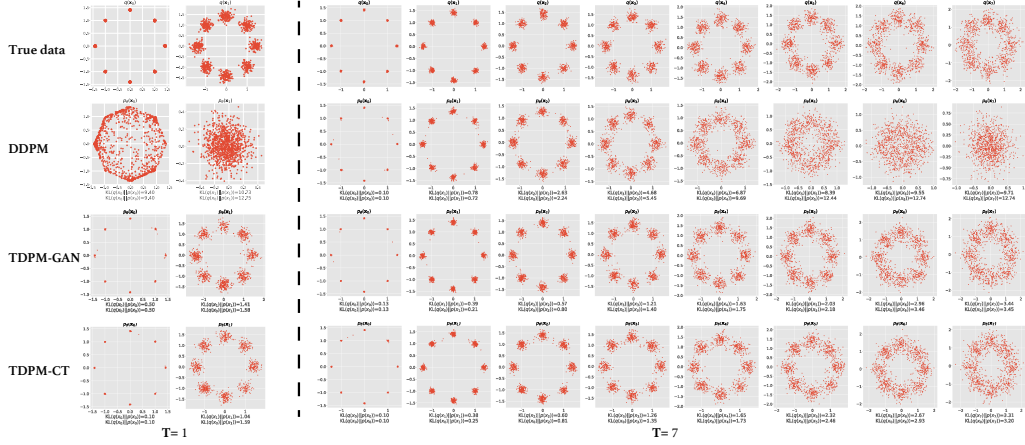


Figure 7: Analogous results to Figure 2 using 8-modal Gaussian data.

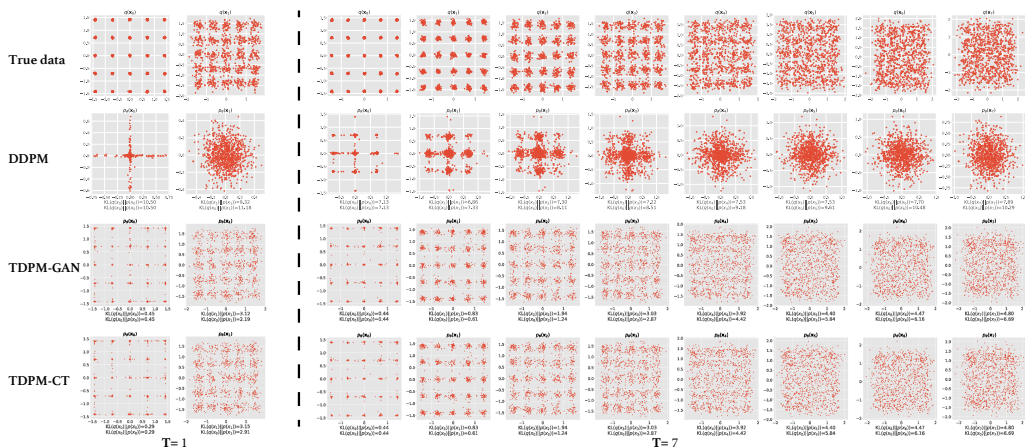


Figure 8: Analogous results to Figure 2 using 25-modal Gaussian data.

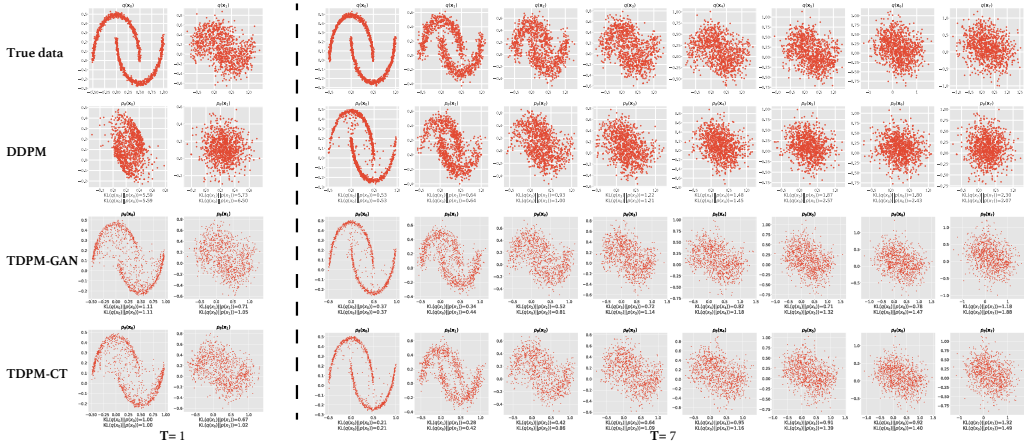


Figure 9: Analogous results to Figure 2 using Double Moons data.

### A.3 Additional results for image experiments

**Sensitivity to noise schedule:** Nichol & Dhariwal (2021) show the noise schedule affects the training of DDPM. Here we examine if TDPM is sensitive to the choice of noise schedule. We compare the linear schedule with cosine schedule, which adds noise in a milder manner. The results on CIFAR-10 are reported in Table 7, which suggest that TDPM is not sensitive to the choice between these two schedules.

Table 7: Ablation study with different noise schedules on CIFAR-10. The number before and after “/” denotes the FID using linear and cosine schedules, respectively.

Model	Steps	FID $\downarrow$ (linear / cosine)
TDPM-GAN	T=99	3.10 / 3.47
TDPM-GAN	T=49	3.30 / 3.16
TDPM-CT	T=99	3.69 / 3.62
TDPM-CT	T=49	3.97 / 3.24

**Additional qualitative results:** From Figure 10-Figure 13, we provide additional results for qualitative justification of TDPM.



Figure 10: Analogous qualitative results to Figure 5 on CelebA-HQ. Produced by TDPM-GAN.

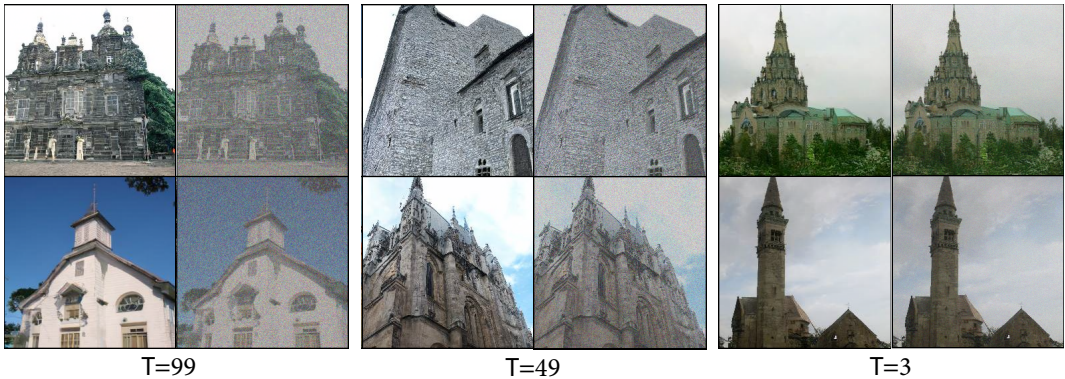


Figure 11: Analogous qualitative results to Figure 5 on LSUN Church. Produced by TDPM-CT.

## B Discussion

**Broader impact:** This paper proposes truncated diffusion probabilistic model as a novel type of diffusion-based generative model. The truncated part can be trained as implicit generative models such as GANs jointly or independently with the diffusion part. The capacities of truncated diffusion probabilistic models are competitive to existing diffusion-based ones and efficiency is largely improved. On the contrary of these positive effects, some negative perspectives could also be seen, depending on how the models are used. One major



Figure 12: Analogous qualitative results to Figure 5 on LSUN Bedroom. Produced by TDPM-CT.



Figure 13: Analogous qualitative results to Figure 5 on CelebA-HQ. Produced by TDPM-CT.

concern is the truncated diffusion technique proposed in this paper could potentially be a way to hack the existing diffusion models if the implicit models are maliciously used to fit the intermediate steps. For example, for some existing diffusion models, for safety concerns, the models capacity to generate private data needs to be locked by hiding the diffusion ending point into an unknown distribution. The technique of TDPM could be used to crack these existing online diffusion models by providing intermediate noisy images or fine-tuning the first few steps with TDPM to unlock the capacity. Besides, the capacity of generating good images can also be misused to generate ill-intentioned images at a much lower cost.

**Discussions:** In this work we mainly focus on reducing the length of the diffusion chain of a finite-time diffusion model. Our model has shown its effectiveness in improving finite-time diffusion models and it is non-trivial to further explore our model on continuous-time diffusion models (Song et al., 2021b). Moreover, while in this paper DDPM is the primary baseline, TDPM can also be built on other recent diffusion models. While  $p_\theta(\mathbf{x}_T)$  is parameterized as an implicit distribution, it can also be formulated as a semi-implicit distribution (Yin & Zhou, 2018), which allows it to be approximated with a Gaussian generator. Xiao et al. (2021b) also present a closely related work. While we share the same spirit to reduce the length of the diffusion chain, these two strategies are not conflicting with each other. In the future work we will look into the integration of these different strategies.

## C Experimental Settings

Below we present our experimental settings in detail.

### C.1 Model architecture

**Generator:** Our generator structure largely follows the U-Net structure (Ronneberger et al., 2015) used in DDPM and DDIM (Ho et al., 2020; Song et al., 2020), which consists of multiple ResNet blocks (He et al., 2016) with Attention blocks (Vaswani et al., 2017) injected in the bottleneck. Please refer to Appendix B of Ho et al. (2020) for more details on these configurations.

A key difference between our model and previous diffusion models is that our model involves an extra implicit generator  $G_\theta$  that takes a latent variable  $\mathbf{z} \sim \mathcal{N}(\mathbf{0}, \mathbf{I})$  as input. However, this does not result in a difference in the generator architecture. We parameterize  $G_\theta$  with the same U-Net architecture for simplicity and the time embedding  $t = T$  is specified to be trained with the implicit loss shown in Equation 9 and Equation 10. We have also tested to remove the impact of time embedding for input at  $t = T$  and found no clear differences. The training of  $G_\theta$  involves a discriminator module.

For our results in Table 5, the generator specially takes a StyleGAN2 architecture Karras et al. (2020b), and this results in an increase of generator parameter. Note that the generator is trained with GAN loss and without specially designed adaptive augmentation Karras et al. (2020a). For the detailed model architecture please refer to the corresponding paper or their Github repository: <https://github.com/NVlabs/stylegan2-ada-pytorch>.

**Discriminator:** Similar to Xiao et al. (2021b), we adopt the discriminator architecture used in Karras et al. (2020b), but without the time step input. The discriminator discriminate  $\mathbf{x}_T$  is from the diffused distribution  $q(\mathbf{x}_T | \mathbf{x}_0)$  or implicit generative distribution  $p_\theta(\mathbf{x}_T)$ . Please refer to Appendix C of Xiao et al. (2021b) for the detailed design.

**Navigator:** Training with  $\mathcal{L}_T^{\text{CT}}$  involves an extra module named navigator (Zheng & Zhou, 2021). We strictly follow the architecture used in Zheng & Zhou (2021), where the navigator is an MLP taking the pairwise feature distance as inputs. The feature is extracted from the layer before the final scalar output. Please refer to their Appendix D for detailed information.

**Architecture for toy experiments:** The generator we use an architecture stacked with 4 linear layers with 128 hidden units. Each intermediate layer is equipped with a time-embedding layer and follows softplus activation. The discriminator and navigator have the same architecture, without time-embedding layers, and using leakyReLU as activation function .

## C.2 Training configurations

**Diffusion schedule:** For all datasets, we deploy a truncated linear diffusion schedule to produce our main results. We obtain the truncated diffusion process by linearly converting the diffusion process in Ho et al. (2020) ( $\beta_1 = 10^{-4}$ ,  $\beta_{T'} = 0.02$ ) with a ratio of  $\frac{T}{T'}$ , where  $T' = 1000$  is the length of a long chain. A simpler equivalent implementation is to first initialize  $\beta_1, \beta_2, \dots, \beta_{T'}$ . Then taking the first  $T$  steps to complete the truncation. In our ablation we have also explored to diffuse with the cosine schedule, whose step segments are not of equal size, but found no significant difference in training and evaluation.

**Optimization:** We train our models using the Adam optimizer (Kingma & Ba, 2015), where most of the hyperparameters match the setting in Xiao et al. (2021b), and we slightly modify the generator learning rate to match the setting in Ho et al. (2020), as shown in Table 8.

We train our models using V100 GPUs, with CUDA 10.1, PyTorch 1.7.1. The training takes approximately 2 days on CIFAR-10 with 4 GPUs, and a week on CelebA-HQ and LSUN Church with 8 GPUs.

Table 8: Optimization hyper-parameters.

	CIFAR10	CelebA	CelebA-HQ	LSUN
Initial learning rate for discriminator	$10^{-4}$	$10^{-4}$	$10^{-4}$	$10^{-4}$
Initial learning rate for navigator (if applicable)	$10^{-4}$	$10^{-4}$	$10^{-4}$	$10^{-4}$
Initial learning rate for generator	$2 \times 10^{-4}$	$2 \times 10^{-4}$	$2 \times 10^{-5}$	$2 \times 10^{-5}$
Adam optimizer $\beta_1$	0.5	0.5	0.5	0.5
Adam optimizer $\beta_2$	0.9	0.9	0.9	0.9
EMA	0.9999	0.9999	0.9999	0.9999
Batch size	128	128	64	64
# of training iterations	800k	800k	0.5M	2.4M(bedroom)/1.2M(church)
# of GPUs	4	8	8	8

## C.3 Evaluation

When evaluating the sampling time, we use models trained on CIFAR-10 and generate a batch of 128 samples. When evaluating the IS, FID, and recall score, following the convention, we use 50k generated samples for CIFAR-10, LSUN-bedroom and LSUN-church, and 30k samples for CelebA-HQ (since the CelebA HQ dataset contains only 30k samples). The recall scores are calculated with the recipe in Kynkänniemi et al. (2019).